Quenching Quantum Tunneling of Magnetization by Turning on the Exchange Coupling and Altering the Bridging Ligand in Heterometallic Octanuclear {$TM^{III}_4Dy^{III}_4$} (TM = Co and Cr) Single-Molecule Magnets

Abstract: We report the synthesis, structural characterization and magnetic properties of two new heterometallic octanuclear coordination complexes containing Co^{III} and Dy^{III} ions. Single crystal X-ray diffraction studies revealed molecular formulae of $[Co^{III}_4Dy^{III}_4(\mu\text{-}OH)_4(\mu_3\text{-}OMe)_4(O_2CC(CH_3)_3)_4(tea)_4(H_2O)_4]\cdot 4H_2O$ (**1**) and $[Co^{III}_4Dy^{III}_4(\mu\text{-}F)_4(\mu_3\text{-}OH)_4(o\text{-}tol)_8(mdea)_4]3H_2O\cdot EtOH\cdot MeOH$ (**2**), with both complexes displaying an identical metallic core topology (tea^{3-} = triply deprotonated triethanolamine; $mdea^{2-}$ = doubly deprotonated N-methyldiethanolamine; o-tol = o-toluate). Furthermore, the theoretical, magnetic and SMM properties of the isostructural complex; $[Cr^{III}_4Dy^{III}_4(\mu\text{-}F_4)(\mu_3\text{-}OMe)_{1.25}(\mu_3\text{-}OH)_{2.75}(O_2CPh)_8(mdea)_4]$ (**3**) are discussed and are compared to a structurally similar complex - $[Cr^{III}_4Dy^{III}_4(\mu_3\text{-}OH)_4(\mu\text{-}N_3)_4(mdea)_4(piv)_4]$ (**4**). Dc and ac magnetic susceptibility data reveal the subtle nature of the SMM characteristics in **1** - **4**, with complexes **2**, **3** and **4** exhibiting SMM behaviour with barrier heights U_{eff} of 39.0 cm^{-1}, 55.0 cm^{-1} and 10.4 cm^{-1} respectively. Complex **1**, on the other hand, does not exhibit slow relaxation of magnetization, above 2 K. To probe the variance in the observed U_{eff} values, CASSCF/RASSI-SO/POLY_ANISO calculations are performed on these complexes to estimate the nature of magnetic coupling and to elucidate the mechanism of magnetic relaxation. Calculations yielded $J_{Dy\text{-}Dy}$ as -1.6, 1.6, and 2.8 cm^{-1} for complexes **1**, **2** and **3**, respectively, while the $J_{Dy\text{-}Cr}$ interaction is estimated to be -1.8 cm^{-1} for complex **3**. The developed mechanism of magnetic relaxation reveals that replacement of the hydroxide ion for fluoride quenches the quantum tunnelling of magnetization (QTM) significantly leading to improved SMM properties for complex **2**, in comparison to **1**. However, the tunnelling of the magnetization at the low lying excited states are still operational for **2**, leading to low temperature QTM relaxation. Replacement of the diamagnetic Co^{III} ions with paramagnetic Cr^{III} leads to Cr^{III}-Dy^{III} coupling, which results in quenching of QTM at low temperatures for complexes **3** and **4**. The best example is found when both Cr^{III} and fluoride are present, as seen for complex **3**, where both the factors additively quench the tunnelling, leading to the observation of highly coercive magnetic hysteresis loops above 2 K ~~a rare observation for a {3d-4f} complex and in fact any complex containing a Ln^{III} ion~~. Here we propose a synthetic strategy to quench the QTM effects in lanthanide based SMMs that differs from existing methods, where often difficult to control parameters such as magnetic coupling is proposed, and the presented strategy is likely to have implications beyond the Dy^{III} single-molecule magnets studied here.

Kuduva R. Vignesh, Stuart K. Langley, Keith S. Murray* and Gopalan Rajaraman*

Introduction

The study and development of molecul~~ar~~e-based magnets have increased markedly over the past twenty years, with discrete molecules exhibiting a wide range of interesting physical properties such as magnetic bistability and an enhanced magnetocaloric effect at cryogenic temperatures.[1] Discrete molecules which exhibit magnetic bistability are termed single-molecule magnets (SMMs), and are isolated as transition or lanthanide ion coordination complexes.[2] These molecules can store digital information by manipulating the orientation of the electrons with a magnetic field, thus offering the potential as the ultimate high density storage device.[3] They rely on creating a large thermal barrier to magnetic reorientation (U_{eff}) which must be sufficiently greater than the thermal energy available in the environment; otherwise no information can be stored. Below their blocking temperature (T_B - the temperature at which digital information can be stored for 100 s) SMMs act as nano-magnets, however the highest blocking temperatures observed to date are 14 K[4] (sweep rate 0.9 mT/s) and 30 K (sweep rate 20 mT/s),[5] for a radical bridged dinuclear Tb^{III} complex and a mononuclear Dy^{III} complex, respectively. While these ultra-low temperatures are not yet viable to see practical application, ongoing research has begun to provide

Prof. Gopalan Rajaraman ,
Department of Chemistry, Indian Institute of Technology Bombay
Powai,Mumbai,Maharashtra,India-400 076
Fax: + 91-22-2576-7152
Email:rajaraman@chem.iitb.ac.in

Kuduva R. Vignesh
IITB-Monash Research Academy,IIT Bombay,
Mumbai,India-400076.

Dr. Stuart K. Langley, School of Science and the Environment,
Division of chemistry, Manchester Metropolitan University,
Manchester, UK.

Prof. Keith S. Murray, School of Chemistry, Monash University,
Victoria,3168, Australia. Email Keith.Murray@monash.edu

Supporting information (figures, tables) for this article is available on the WWW under http:/www.chemeurj.org/ or from the author

guidelines (synthetic and theoretical) on how to design and improve upon current materials.[6]

One such suggestion was the use of lanthanide ions towards the synthesis of SMMs, lanthanides being not widely used until recently.[2, 7] The development of lanthanide based SMMs over the past five years has resulted in great gains in the magnitude of the thermal energy barrier (U_{eff}) and therefore the blocking temperature.[2b, 8] A number of groups[9] has shown that the U_{eff} parameter can be "tailored" by selection of ligands and the coordination geometry around the lanthanide ion.[10] This allows for a rational design approach which allows for a greater control of properties, such designs being distinctly lacking for transition metal based SMMs.[2b, 11] Principles have been developed to improve the thermal barrier and relaxation times of various complexes by modifying the coordination environment of the lanthanide ion in several SMMs.[12] We have recently shown this to be the case for a series of heterometallic $\{Co^{III}_2Dy^{III}_2\}$ tetranuclear complexes, whereby modifying chemically the terminally coordinated ligands revealed U_{eff} values ranging from ~~14~~ 10 – ~~170~~ 97 cm^{-1}~~K~~.[13] Incorporation of diamagnetic elements in cluster aggregates has also been found to enhance U_{eff} significantly, for example in a series of $\{Zn^{II}Dy^{III}\}$ SMMs.[10b, 14]

Following on from our studies with $\{Co^{III}_2Dy^{III}_2\}$ SMM complexes,[13] which focussed on modifying the terminal ligands coordinated to the Dy^{III} ion, we have shown that the SMM properties can also easily be enhanced by modification of a single bridging element in a heterometallic octanuclear $\{Cr^{III}_4Dy^{III}_4\}$ complex.[15] We have continued this synthetic modification approach and herein we report the molecular structures, magnetic data and theoretical characterization of two new heterometallic 3d-4f SMM complexes of formulae $[Co^{III}_4Dy^{III}_4(\mu\text{-}OH)_4(\mu_3\text{-}OMe)_4(O_2CC(CH_3)_3)_4(tea)_4(H_2O)_4]\cdot 4H_2O$ (**1**) and $[Co^{III}_4Dy^{III}_4(\mu\text{-}F)_4(\mu_3\text{-}OH)_4(o\text{-}tol)_8(mdea)_4]\cdot 3H_2O\cdot EtOH\cdot MeOH$ (**2**) (tea^{3-} = triply deprotonated triethanolamine, $mdea^{2-}$ = doubly deprotonated N-methyldiethanolamine and o-tol(H) = *ortho*-toluic acid). Both complexes display the same metallic topology, but importantly are isolated with different bridging ligands ($\mu\text{-}OH^-$ vs $\mu\text{-}F^-$). As a consequence of this we find that compounds **1** and **2** display significantly different magnetization relaxation dynamics. We have performed an in depth *ab initio* and density functional theory (DFT) studies to explain these observations. To fully comprehend the role of bridging ligand and the diamagnetic ions, we have extended our theoretical studies to the above mentioned structurally analogous octanuclear complex - $[Cr^{III}_4Dy^{III}_4(\mu\text{-}F_4)(\mu_3\text{-}OMe)_{1.25}(\mu_3\text{-}OH)_{2.75}(O_2CPh)_8(mdea)_4]$ (**3**), reported by us,[15] and compared the results with another structurally similar complex, $[Cr^{III}_4Dy^{III}_4(\mu_3\text{-}OH)_4(\mu\text{-}N_3)_4(mdea)_4(piv)_4]$ (**4**), reported by Powell and co-workers, which provided a similar F^- vs. N_3^- analogy.[16]

Experimental Section

General Information

The reactions were carried out under aerobic conditions. Chemicals and solvents were obtained from commercial sources and used without further purification.

Synthesis of $[Co^{III}_4Dy^{III}_4(\mu\text{-}OH)_4(\mu_3\text{-}OMe)_4(O_2CC(CH_3)_3)_4(tea)_4(H_2O)_4]\cdot 4H_2O$ (1).

$Co(BF_4)_2\cdot 6H_2O$ (0.34 g, 1 mmol) and $Dy(NO_3)_3\cdot 6H_2O$ (0.22 g, 0.5 mmol) were dissolved in MeCN (20 mL), followed by the addition of triethanolamine (0.14 mL, 1 mmol), pivalic acid acid (0.10 g, 1.0 mmol) and triethylamine (0.55 mL, 4.0 mmol). This resulted in a dark green solution, which was stirred for 4 hours. After this time the solvent was removed to give a green oil. The oil was re-dissolved in MeOH and layered with diethylether (Et_2O). Within 4-5 days' green crystals of **1** had appeared, in approximate yield of 34 % (crystalline product). Calculated (found) for **1**: $Co_4Dy_4C_{48}H_{108}O_{36}N_4$: C, 26.16 (26.45); H, 4.94 (4.87); N, 2.54 (2.34).

Synthesis of $[Co^{III}_4Dy^{III}_4(\mu\text{-}F)_4(\mu_3\text{-}OH)_4(o\text{-}tol)_8(mdea)_4]\cdot 3H_2O\cdot EtOH\cdot MeOH$ (2).

$Co(NO_3)_2\cdot 6H_2O$ (0.29 g, 1 mmol) and $Dy(NO_3)_3\cdot 6H_2O$ (0.22 g, 0.5 mmol) were dissolved in MeCN (20 mL), followed by the addition of N-methyldiethanolamine (0.12 mL, 1 mmol), *ortho*-toluic acid (0.13 g, 1 mmol), sodium fluoride (0.08 g, 2 mmol) and triethylamine (0.55 mL, 4.0 mmol). This resulted in a dark green solution which was stirred for 4 hours. After this time the solvent was removed resulting in a green oil. The oil was re-dissolved in MeOH/EtOH (1:1) and layered with diethylether (Et_2O). Within 8-10 days' green crystals of **2** had appeared, in approximate yield of 45 % (crystalline product). Calculated (found) for **2**: $Co_4Dy_4C_{87}H_{120}O_{33}F_4N_4$: C, 38.54 (38.21); H, 4.46 (4.21); N, 2.07 (2.14), F, 2.80 (2.56).

X-ray Crystallography. X-ray measurements for **1** were performed at 123(2) K using a Bruker Smart Apex X8 diffractometer with Mo Kα radiation. The data collection and integration were performed within SMART and SAINT+ software programs, and corrected for absorption using the Bruker SADABS program. Measurements for compound **2** were performed at 100(2) K at the Australian synchrotron MX1 beam-line.[17] The data collection and integration were performed within Blu-Ice[18] and XDS[19] software programs. Compounds **1** and **2** were solved by direct methods (SHELXS-97),[20] and refined (SHELXL-97)[21] by full least matrix least-squares on all F^2 data.[22] Crystallographic data and refinement parameters for **1** and **2** are summarized in Table S1. Crystallographic details are available in the Supporting Information (SI) in CIF format. CCDC numbers 1510015 (**1**) and 1510016 (**2**). These data can be obtained free of charge from the Cambridge Crystallographic Data Centre via www.ccdc.cam.ac.uk/data_request/cif.

Magnetic Measurements. The magnetic susceptibility measurements were carried out on a Quantum Design SQUID magnetometer MPMS-XL 7 operating between 1.8 and 300 K for dc-applied fields ranging from 0 – 5 T. Microcrystalline samples were dispersed in Vaseline in order to avoid torquing of the crystallites. The sample mulls were contained in a calibrated gelatine capsule held at the centre of a drinking straw that was fixed at the end of the sample rod. Alternating current (ac) susceptibility measurements were carried out under an oscillating ac field of 3.5 Oe and frequencies ranging from 0.1 to 1500 Hz.

Computational details

Using MOLCAS 7.8,[23] *ab initio* calculations were performed on the Dy^{III} ions and the Cr^{III} ions using the single crystal structure data. The employed methodology and basis sets are described in detail in ESI.

Moreover, these computed spin-orbit (SO) states have been considered into the SINGLE_ANISO[24] program to compute the *g*-tensors. Crystal-field parameters have been extracted using the SINGLE_ANISO code, as implemented in MOLCAS 7.8. The magnetic exchange interactions (*J*)

have been computed between Dy^{III} ions (J_1) within each complex by fitting with the experimental data using POLY_ANISO.[25] The Cr-Dy(J_2) and Cr-Cr(J_3) interactions have also been computed for complex **3** (See the magnetic exchange pathways in Figure S1).

To further validate the exchange coupling obtained from the POLY_ANISO program we have also computed the magnetic exchange within density functional formalism. The DFT calculations combined with the Broken Symmetry (BS) approach[26] has been employed to compute the *J* values (see ESI for details). The BS method has a proven record for yielding good numerical estimates of *J* constants for a variety of coordination complexes,[27] including dinuclear molecules,[28] Gd complexes[29] and large polynuclear complexes.[6d, 27b, 30]

Results and discussion

Synthesis and crystal structures

Complex **1**, $[Co^{III}_4Dy^{III}_4(\mu\text{-}OH)_4(\mu_3\text{-}OMe)_4(O_2CC(CH_3)_3)_4(tea)_4(H_2O)_4]\cdot 4H_2O$, was synthesised by reacting $Co(BF_4)_2\cdot 6H_2O$and $Dy(NO_3)_3\cdot 6H_2O$, with triethanolamine ($teaH_3$), pivalic acid and triethylamine in methanol. In an attempt to isolate an analogous complex with the inclusion of fluoride bridging ligands, in order to modify the magnetic properties, we attempted a variety reactions using various reagents and conditions. We found we could isolate one pseudo isostructural complex with the same metallic topology, $[Co^{III}_4Dy^{III}_4(\mu\text{-}F_4)(\mu_3\text{-}OH)_4(O\text{-}tol)_8(mdea)_4]\cdot 3H_2O\cdot EtOH\cdot MeOH$ (**2**), using NaF as a source of fluoride, with N-methyldiethanolamine (in place of triethanolamine), *ortho*-toluic acid (in place of pivalic acid) and acetonitrile as the solvent. Single crystals of **1** were grown from a methanolic solution, while a MeOH/EtOH mixture was used for **2**.

Single crystal X-ray analysis revealed that **1** and **2** are heterometallic octanuclear complexes (Figure 1, top left (**1**) and top right (**2**)), which crystallize in the tetragonal and monoclinic space groups, *I-42m* and *P2n*, respectively. The asymmetric unit of **1** consists of one quarter of the molecule, while the asymmetric unit of **2** consists of the whole molecule. The metallic core arrangement is identical for both molecules. Each consist of four Co^{III} and four Dy^{III} ions, with an inner Dy^{III}_4 square (Dy…Dy distance of 3.83 Å (**1**) and average Dy…Dy distance of 3.83Å (**2**)) surrounded by four Co^{III}_4 ions. Each Co^{III} ion lie alternately, above and below the plane of the $\{Dy_4\}$ square,capping each edge (Figure 1, bottom right) (Co…Co distance of 6.64Å (**1**) and average Co…Co distance of 6.56 Å (**2**)). For comparitive purposes the molecular structure of the $\{Cr^{III}_4Dy^{III}_4\}$ analogue, **3**, is shown in Figure 1, bottom left. The valency of the Co ions were confirmed from BVS calcualtions[31] and from charge balance considerations (ESI Tables S2, S3). The four Dy^{III} ions are bridged by four μ atoms and four μ_3 groups. Each μ_3 ligand also bridges to a single Co^{III} ion. The μ atoms are assigned as hydroxide (OH^-) for **1** and fluoride (F^-) for **2**. Evidence for fluoride is provided by elemental analysis and close inspection of the crystallographic data. The μ_3 bridges are found to be methoxide (MeO^-) for **1** and hydroxide (OH^-) for **2**. For both complexes each doubly deprotonated aminepolyalcohol ligand coordinates via the N- and two O-atoms to an"outer" Co^{III} ion, two O-atoms then bridge froma Co^{III} to a Dy^{III} ion. For **1** the third alcohol arm chelates to the Co^{III} ion, with the pivalate ligands each bridging a Co^{III} to a Dy^{III} ion. The X-ray analysis reveals disorder in the crystal for **1** (See ESI and Figure S1). For **2**, however, due to the absence of the third alcohol arm no disorder is found, with eight carboxylate ligands bridging the Co^{III} and Dy^{III} ions. The four Dy^{III} ions for **1** and **2** are eight coordinate with biaugmented trigonal prismatic geometries (see magnetic analysis, *vide infra*), with an average Dy^{III}-L bond distance of 2.322 and 2.334 Å, respectively. The four Co^{III} ions, for both **1** and **2** are six coordinate with octahedral geometries, with an average Co^{III}-L bond distance of 1.907 and 1.908 Å, respectively. Selected bond lengths and bond angles are given in Table S4.

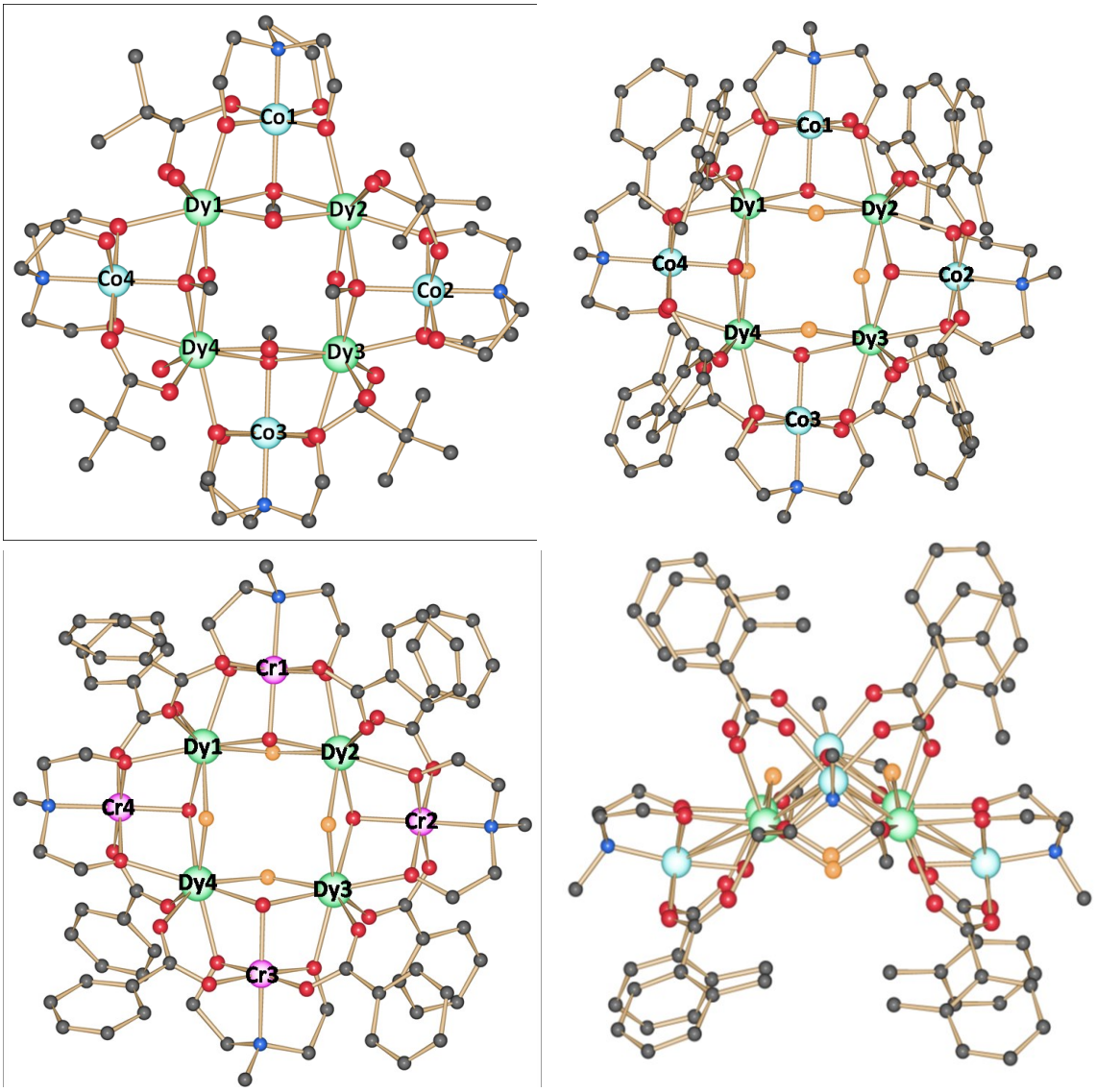

Figure 1. Molecular structures of complex **1** (top left), **2** (top right), **3** (bottom left) and a view along the plane of the {Dy_4} square of **2** (bottom right). The disordered, solvent and H atoms are omitted for clarity. Colour scheme; Co^{III}, light blue; Cr^{III}, pink; Dy^{III}, purple; O, red; N, blue; C, light grey; F, orange.

The key chemical features are the replacement of the hydroxide (μ-OH^-) ions in **1** for fluoride (μ-F^-) ions in **2**. We see later that this simple chemical modification impacts the magnetic properties and single-molecule magnet behaviour significantly.

Magnetic properties

Direct current magnetic susceptibility measurements

In order to probe the magnetic properties, direct current (dc) magnetic susceptibility measurements were performed on polycrystalline samples of **1** and **2** in the temperature range 2 – 300 K, using an applied magnetic field of 1 T. The plots of $\chi_M T$ (where χ_M is the molar magnetic susceptibility) *versus* T for **1** and **2** (Figure 2 and S2), reveal room temperature $\chi_M T$ values of 56.68 and 56.27 cm^3 K mol^{-1}, respectively. These values are in good agreement with that expected of 56.68 cm^3 K mol^{-1} for four Dy^{III} ions (S = 5/2, L = 5, $^6H_{15/2}$, g = 4/3, C= 14.17 cm^3 K mol^{-1}), that are non-interacting.[32] The four Co^{III} ions have the low spin d^6 electronic configuration and are therefore diamagnetic (apart from a small 2nd order Zeeman contribution), not contributing to the magnetic susceptibility.[33] Both compounds display similar profiles, where the $\chi_M T$ product decreases gradually between 300 -50 K upon reduction of the temperature, due to the depopulation of the Stark sub-levels of the Dy^{III} ions due to crystal-field effects. Below 50 K, the $\chi_M T$ values fall rapidly,

reaching values of 18.72 and 19.61 cm^3 K mol^{-1}, at 2 K, for **1** and **2**, respectively. These plot profiles indicate the likelihood of weak antiferromagnetic exchange interactions occurring between the Dy^{III} ions and/or a large single ion anisotropy. The magnetic exchange interactions for **1** and **2** are discussed in detail below.

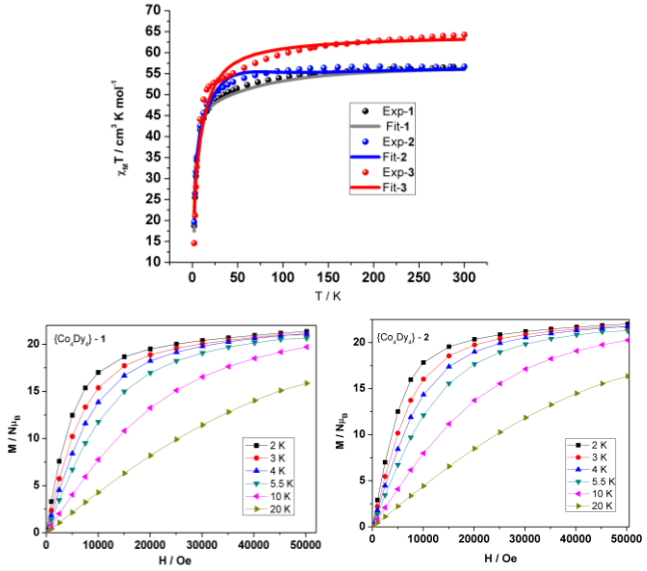

Figure 2. (top) The measured and the fitted $\chi_M T$ versus T plots for **1**, **2** and **3** with a dc field of 1 T; Plots of M versus H isotherms for **1** (bottom left) and **2** (bottom right) at 2, 3, 4, 5.5, 10 and 20K.

Isothermal magnetization (M) measurements for **1** and **2**, plotted as a function of the magnetic field (H) are shown in Figure 2, bottom. The samples display similar profiles with a rapid increase in magnetization below 2 T, before following a more gradual linear-like increase, without saturating, thus signifying a significant anisotropy and/or low lying excited states are present. This is further supported by the 2 K magnetization values of 21.35 and 22.01 $N\mu_B$ for **1** and **2**, respectively.

Alternating current magnetic susceptibility measurements

To probe for slow magnetic relaxation and SMM behaviour the magnetization dynamics were investigated for **1** and **2** via alternating current (ac) susceptibility measurements as a function of both temperature and frequency. Initially a 3.5 Oe ac field was employed, with a zero static dc field. For compound **1** (Figure 3, top left) frequency dependent "tails" in the out-of-phase susceptibility (χ_M") *versus* temperature plots, are observed, below 3 K, with the peak maxima falling below the operating temperature of the SQUID magnetometer. This signifies a small anisotropy barrier and/or the presence of fast QTM. In many lanthanide containing SMMs, QTM is fast but can be quenched via the application of a static dc magnetic field. We therefore probed the effect that a static magnetic field has on the relaxation time. Upon application of a 3000 Oe dc magnetic field we find that the out-of-phase signals shift to higher temperatures, indicating the QTM is quenched to some extent, however, the peak maxima are obscured by a second increase at the lowest temperatures, indicating the QTM pathway is still active (Figure S3).

For compound **2**, however, frequency dependent out-of-phase signals are observed (Figure 3, top right) below 12 K in zero applied dc magnetic field. An initial increase in the χ_M" signal is found at temperatures below ~16 K, a much greater temperature than for **1** (< 3 K). These signals are, however, obscured by a larger increase of χ_M" at temperatures below 6 K which do not reach a maximum above 1.8 K. This second relaxation at low temperatures is indicative of a QTM relaxation process. Due to the presence of QTM we performed measurements in the presence of an applied dc magnetic field of 5000 Oe in order to quench the QTM assisted relaxation. The χ_M" versus T plot (Figure 3, bottom right), however, reveals a more complicated picture. It shows the likelihood of three relaxation processes, two thermally activated, in addition to an under barrier process (QTM). This can best be observed at 1488 Hz (Figure 3, bottom left, inset). At this frequency, as the temperature is reduced, peak maxima in χ_M" are found at ~12 K and ~5 K, before a further increase at the lowest temperatures.In an attempt to extract relaxation times for **2**, we performed variable frequency (0.1 – 1500 Hz) studies using a 3.5 Oe oscillating ac field, at fixed temperatures (2 – 11 K), with a zero static dc field. The χ_M" *versus* frequency plots (Figure 3, bottom right), as expected, reveal multiple relaxation pathways – at least three are identifiable. This is evident at the lowest temperatures (2 – 5 K) and from the Cole-Cole plots (χ_M' *versus* χ_M", Figure 4, inset) which reveal several fused semi-circular profiles. From the data obtained it is possible to extract/extrapolate relaxation times for the slowest process (the peaks which correspond to the lowest frequency at a fixed temperature). The susceptibility maxima are dependent on temperature indicating a thermally activated process at the temperatures probed. Plots of ln(τ) versus 1/T are linear between 8 – 10.5 K (Figure 4), however, below 7 K the the relaxation times deviate from linearity (Figure S4). This confirms that a thermally activated Orbach process is operative at higher temperatures, with the low temperature deviation suggestive of a crossover towards a QTM relaxation mechanism. Fitting the data to the Arrhenius law [$\tau = \tau_o exp(U_{eff}/k_B T)$] in the linear (thermally activated) region yields a significant effective anisotropy barrier to magnetization reversal of U_{eff} = 39 ± 1 cm^{-1}, with τ_o= 1.0 x 10^{-6} s (R = 0.99). Relaxation data for the second and third processes could not be extracted from the data collected.

A comparison of compounds **1** and **2** reveal strikingly different magnetization dynamics. For **1** (H_{dc} = 0 Oe), no maxima in the χ_M" signals are observed above 2 K, whereas maxima (multiple relaxation pathways at the lowest temperatures) are found for compound **2**, up to 12 K. In essence we observe a significant increase in the magnetic relaxation time at the temperatures probed for compound **2**. This observation is important as the difference between the two molecules is minor, consisting of a small chemical modification of the first coordination sphere to the Dy^{III} ions - the substitution of the μ_2-OH^- ion for μ_2-F^-. This suggests, strongly, that the chemical modification of existing clusters can result in longer relaxation times and, thus, relatively, better performing SMMs.

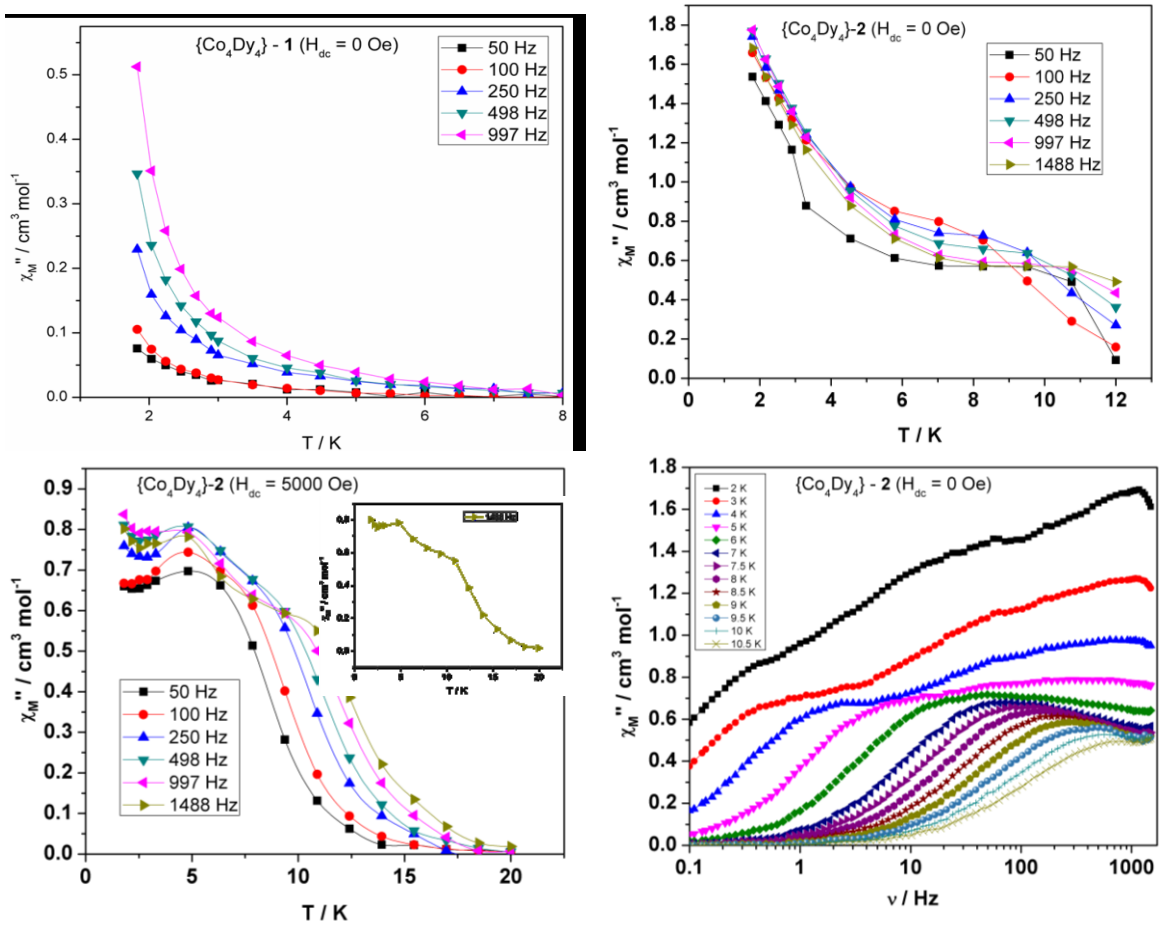

Figure 3. (top left) Plot of χ_M'' versus T at the frequencies indicated for **1** (H_{dc} = 0 Oe); (top right) Plot of χ_M'' versus T at the frequencies indicated for **2** (H_{dc} = 0 Oe); (bottom left) Plot of χ_M'' versus T at the frequencies indicated for **2** (H_{dc} = 5000 Oe), inset temperature dependence of χ_M'' at 1488 Hz; (bottom right)Plot ofχ_M'' versus frequency ν at the temperatures indicated for **2** (H_{dc} = 0Oe).

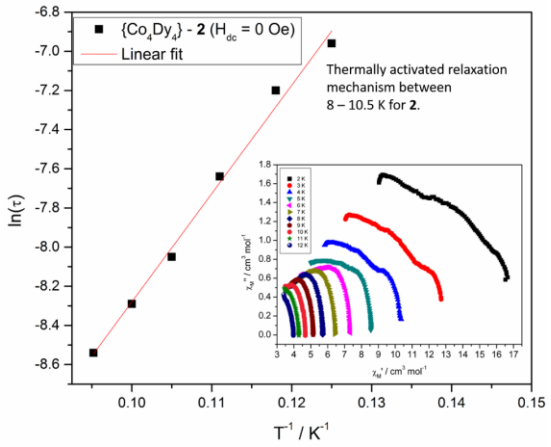

Figure 4. Magnetization relaxation time (τ) plotted as ln(τ) *versus* T^{-1} for compound **2**. The solid red line represents a fit to the Arrhenius law in the thermally activated regime. (inset) Cole-Cole plots of **2** at temperatures between 2 and 12 K.

A similar situation was recently reported for two analogous heterometallic octanuclear $\{Cr^{III}_4Dy^{III}_4\}$ complexes **3** and **4**.[15-16] The metallic core topology of **3** and **4** is identical to that found for **1** and **2** (Figure 1). The magnetic measurements revealed that complex **4** displays SMM behaviour with relatively fast relaxation times at ~ 2 K, whereas upon modification of the bridging ligands – the replacement of N_3^- (**4**) for F-donor (**3**) ligands resulted in a significant increase in relaxation times for **3** at the same temperature. It was reported that **4** displayed a U_{eff} value of 10.4 cm^{-1}, whereas the U_{eff} value for **3** was 55.0 cm^{-1}. More interestingly, the relaxation time for **3** was long enough to observe highly coercive magnetic hysteresis loops at temperatures below 3.5 K (Figure S5).[15] With these results in mind it is therefore important to elucidate the factors that are responsible for the observation of longer relaxation times (at a particular temperature) in near identical complexes. We have therefore performed *ab initio* calculations on the two $\{Co^{III}_4Dy^{III}_4\}$ complexes **1** and **2** to determine such factors. We have also performed a theoretical analysis on the $\{Cr^{III}_4Dy^{III}_4\}$ analogue **3** and compared the data with previously reported results for complex **4**.

Theoretical studies

The magnetic properties of **1**, **2** and **3** have been studied theoretically using *ab initio* CASSCF+RASSI-SO calculations employing the SINGLE_ANISO routine to compute the anisotropy of the individual Dy^{III} and Cr^{III} ions and POLY_ANISO to employ the Lines model to fit the susceptibility/temperature plots. First we discuss the magnetic anisotropy at the single Dy^{III} ion level and the corresponding single ion relaxation mechanism. We will then expand the discussion to include the exchange coupling between the Dy^{III}....Dy^{III} and Cr^{III}...Dy^{III} ions for **1** – **3**, and develop a new exchange coupled relaxation mechanism, which is found to be in good agreement with the experimental data.

Mechanism of Magnetic Relaxation: Single ion Paradigm: Since the Co^{III} ions are diamagnetic in **1** and **2**, the SMM behaviour originates from the Dy^{III} anisotropy alone. Thus we have explored the anisotropy of Dy^{III} for all four centres in **1** and **2** using *ab initio* methods. Whereas in **3**, we have explored the anisotropy of all the ions (Cr^{III} and Dy^{III}). Analysis of the coordination environment of each Dy^{III} ion for **1** – **4** utilizing the SHAPE program[34] revealed there are two types of non-equivalent Dy^{III} sites in **1**–**3**, (Dy1 and Dy2, Figure 1), whereas in **4**, all Dy^{III} ions are equivalent. The geometry of each Dy^{III} ion for **1** – **3**, is best described as an biaugmented trigonal prism. A deviation, with respect to an ideal biaugmented trigonal prism of 0.6, 1.3 and 1.07 for (Dy1 and Dy4) and 0.8, 1.0 and 1.05 for (Dy2 and Dy3) is found for **1**, **2** and **3**, respectively. For **4** all Dy^{III} ions are found in a square antiprismatic geometry. A deviation of 0.5 for each Dy^{III} ion is observed with respect to an ideal square antiprismatic geometry. To fully understand the single-ion relaxation process, we have undertaken CASSCF+RASSI-SO calculations to compute the anisotropy of the individual Dy^{III} ions using MOLCAS 7.8 (see ESI for computational details). The calculated anisotropic *g* values are listed in Tables 1, S6, S9 and S13 and their anisotropy orientations are shown in Figure 5. It is found that the sites [Dy1 and Dy4] and [Dy2 and Dy3] possess similar anisotropic parameters (see Table 1), as a reflection of the SHAPE analysis. The computed energies of the eight low-lying Kramer's doublets (KDs) also reflect that there are two types of Dy^{III} ions for **1** - **3** (see Tables S5, S8 and S11). The energy gap between the ground and the first excited state KDs are found to be 4.9 cm^{-1} and 8.4 cm^{-1} for Dy1 and Dy2, respectively in **1**, 42.9 cm^{-1} and 68.9 cm^{-1} for Dy1 and Dy2, respectively in **2** and 40.6 cm^{-1} and 25.6 cm^{-1} for Dy1 and Dy2, respectively, in **3**. For **4**, with only one equivalent Dy^{III} ion the ground to first excited state gap was reported to be 23.3 cm^{-1}.[16] These results show that the ground to first excited state energy gaps are significantly larger for complexes **2** and **3**, compared to complex **1**. Complex **4** is intermediate. Since the energy gap is correlated to the crystal-field splitting energy, this suggests relatively weaker splitting of the m_J levels in **1** compared to **2**–**4**.

For complex **1**, all the Dy-O distances are in the range of 2.32 - 2.44 Å except for the Dy-O(H) distances which are shorter (2.22 Å). As the hydroxide ligands are bridging between Dy^{III} ions, and because of the square $\{Dy^{III}_4\}$ topology they lie at a right angle to each other at the Dy^{III} site. These hydroxide bridges are found to have large negative Mulliken charges forcing the β-electron (spin-down) of the Dy^{III} ion to lie perpendicular to these bridges to minimize electrostatic repulsion (See Figure 5a). This forces the g_{zz} axis to be perpendicular to the β-electron density, i.e. lies along one of the Dy-OH axis (See Figure 6a). The proximity of the diamagnetic Co^{III} ion to the two of alkoxide bridges enhances the negative charge on these oxygen atoms as a strong polarization from a +3 cation is expected. These methoxide bridges therefore have very large negative charges compared to the hydroxide bridges (See Figure 5a), further enforcing the g_{zz} axis to lie along the hydroxide bridge. The magnetic anisotropy of the oblate Dy^{III} ion arises due to crystal field splitting of the m_J levels as this is correlated to the nature of the interactions. Although the stronger axial interaction is exerted by the hydroxide ensuring stabilization of $m_J = \pm 15/2$ as the ground state, as the two hydroxide bridges are at a right angle to each other, this results in the stabilization of $m_J = \pm 1/2$ as the first excited state. The minor variation in the ground to first excited state energy gap between Dy(1) and Dy(2) are due to minor structural alterations as described by the SHAPE analysis.

Table 1. *Ab Initio* computed ground state *g*-tensors for each Dy^{III} centre in **1**–**4**.

Com-plex		Dy1	Dy2	Dy3	Dy4
1	g_x	0.9705	0.5419	0.5806	0.1004
	g_y	6.6958	1.8736	2.1638	6.3070
	g_z	13.3107	18.0245	17.7693	13.4578
2	g_x	0.0098	0.0039	0.0028	0.0009
	g_y	0.2842	0.0576	0.0360	0.2142
	g_z	19.4753	19.6320	19.6578	19.3850
3	g_x	0.0626	0.1995	0.1862	0.0653
	g_y	0.1349	1.0026	0.9827	0.1426
	g_z	19.6892	18.0941	18.0411	19.5603
4	g_x	1.6671			
	g_y	5.8397			
	g_z	14.4193			

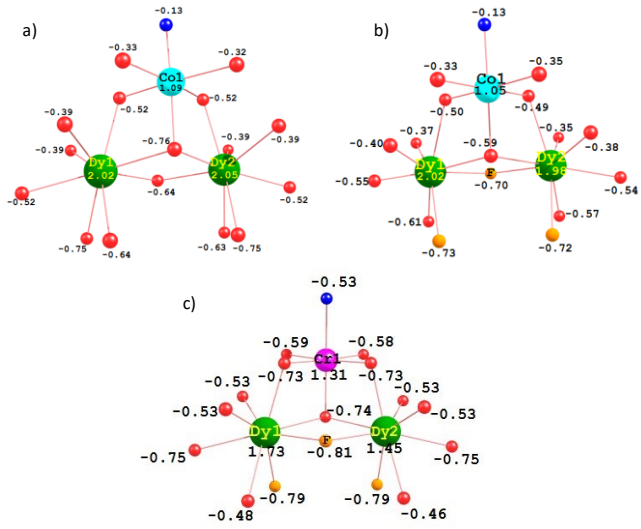

Figure 5. DFT-computed Mulliken charges on the donor atoms of complex (a) **1**, (b) **2** and (c) **3**.

In complex **2** the bridging hydroxide (μ-OH^-) ligands are replaced by fluoride (μ-F^-) ions. The Dy^{III}-O distances found in complex **2** are very similar to that of complex **1**. The

average Dy^{III}-F distances are found to be 2.247 Å. Each fluoride ion is found to possess strong negative charge, enforcing g_{zz} to pass along the Dy^{III}-F bond (See Figure 6b). As explained above, because two fluoride ions are bonding to the Dy^{III} ion at a right angle to each other, the $m_J = \pm 1/2$ is stabilized as the first excited state. As the fluoride ion is a harder base compared to hydroxide, it therefore exerts a stronger electrostatic repulsion pushing the first excited state higher in energy by 42.9 cm^{-1} and 37.7 cm^{-1} for Dy1 and Dy2, compared to **1**. Another important reason for the larger gap in **2** compared to **1** is due to the smaller negative charge found on the bridging oxygen atom connecting the two Dy^{III} ions (see Figure 5b). In complex **1**, these are alkoxide bridges, possessing a significantly large negative charge on the equatorial plane (see Figure 5a), while in complex **2** the hydroxide ions reduce this repulsion considerably. Complex **3** possesses one hydroxide oxygen and one alkoxide oxygen *trans* to each other possessing very large negative charges (See Figure 5c), this favours the g_{zz} axis to lie along this axis (see Figure 6c) leading to a larger ground-first excited state gap compared to complex **1**.

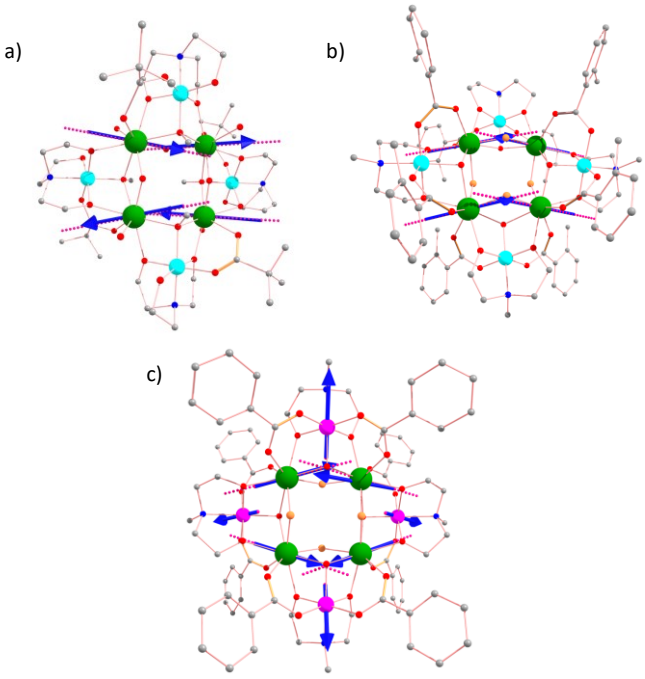

Figure 6. The directions of the local anisotropy axes in the ground Kramer's doublet on each Dy^{III} site (blue arrows) in **1 – 3** along with the anisotropy axes of Cr^{III} ions in **3**, (c).

The computed *g*-anisotropies of complexes **1** - **4** are shown in Table 1. In all cases $m_J = \pm 15/2$ is found to be stabilized as the ground state as the axial interactions are stronger compared to equatorial interaction. However, in complex **1** a significant transverse anisotropy is present for the ground state KD due to strong mixing of $m_J = \pm 15/2$ with $m_J = \pm 1/2$ states (see Figure 7a and 7b). A similar situation is encountered for **4**.[16] The transverse component for the Dy2 (and Dy3) ions are considerably less than Dy1 (and Dy4), due to the larger energy gap between the $m_J = \pm 15/2$ and the $m_J = \pm 1/2$ states.

Due to the significant transverse anisotropy, and the low lying first excited state for **1**, it is not expected to exhibit magnetization blockade at the single ion level as revealed by the experiments. For **2** and **3**, on the other hand, the g_z values are almost purely axial in nature. This is because the mixing of the $m_J = \pm 15/2$ state, with the excited states are significantly reduced due to the increased energy gap between the ground KD and the excited state KD. More importantly, as the first excited state KD is significantly higher in energy this suggests possible magnetization blockade at the single-ion level.[35]

To determine relaxation processes associated with single-ion Dy^{III} anisotropy, the mechanisms of magnetic relaxation are computed and these are shown in Figure 7. In **1**, the ground state tunnelling probability is large for all Dy^{III} ions leading to no magnetization blockade, as expected (see Figure 7a and 7b). Whereas in **2**, the ground state tunnelling probability is smaller relative to **1** (0.64 X 10^{-1} and 0.1 x 10^{-1} μ_B), but not sufficiently negligible to quench the QTM completely at the ground state level i.e. if an isostructural $\{Co^{III}_4Dy^{III}La^{III}_3\}$ complex is prepared, it is unlikely to show SMM behaviour due to the large ground state tunnelling probability (See Figure 7c and 7d). However, if we consider relaxation beyond a single-ion mechanism and factors such as Dy^{III}...Dy^{III} exchange coupling could quench the observed QTM effects leading to a possible magnetization blockade (*vide infra*). In **3**, the tunnelling probability at the single ion level is larger than **2**, and the calculations again predict the absence of SMM behaviour (See Figure 7e and 7f). This is however contrary to what is observed from experimental measurements.[15] To explain the data, we must take into account the Dy^{III}...Dy^{III} and Cr^{III}....Dy^{III} exchange coupling. CASSCF calculations performed for the Cr^{III} single ions yield isotropic *g*-tensors (see Table S13 in ESI) and axial zero-field splitting parameter values of -0.2 cm^{-1} for Cr1 and -0.3 cm^{-1} for Cr2, Cr3 and Cr4, with a small E/D ratio. These values are too small to significantly influence the magnetic anisotropy of the Dy^{III} centres.

Mechanism of Magnetic Relaxation: Polynuclear Paradigm: As illustrated above, the single ion Dy^{III} anisotropy and the developed mechanism of relaxation does not rationalize the observation of slow magnetic relaxation in complexes **1** – **3**. To gain insight into the mechanism of relaxation, a polynuclear mechanism needs to be developed, incorporating the exchange coupling between the paramagnetic centres. This has been performed using the POLY_ANISO program which employs the Lines model to fit the susceptibility data using the *ab initio* computed parameters of the Dy^{III}/Cr^{III} single ion. This has successfully been employed to extract a good numerical estimate of magnetic exchange parameters (*J* values) in several earlier instances.[13e, 13f, 36] The exchange Hamiltonian adapted for complexes **1**, **2** and **3** is given below (Eq. 2) along with the exchange topology diagram shown in Figure 8.

$$\widehat{H_{ex}} = - \sum_{i=1}^{3} J_i . S_i . S_{i+1} \quad \text{.....Eq. 2}$$

(here $J_i = J_i^{exch}$; i.e. J_i are the fitted J_i^{exch} parameters; this describes the interaction between all the neighboring metal centers.)

Due to the high symmetry found in complexes **1** and **2**, the Dy^{III}-O-Dy^{III} and Dy^{III}-F-Dy^{III} angles are identical for all Dy^{III}-Dy^{III} pairs. We have therefore employed a single exchange

interaction (J_1) for these two complexes. For **3** two additional magnetic exchange parameters Dy^{III}-Cr^{III} (J_2) and Cr^{III}-Cr^{III} (J_3) are employed (see computational details and Figure 8).[16, 37]

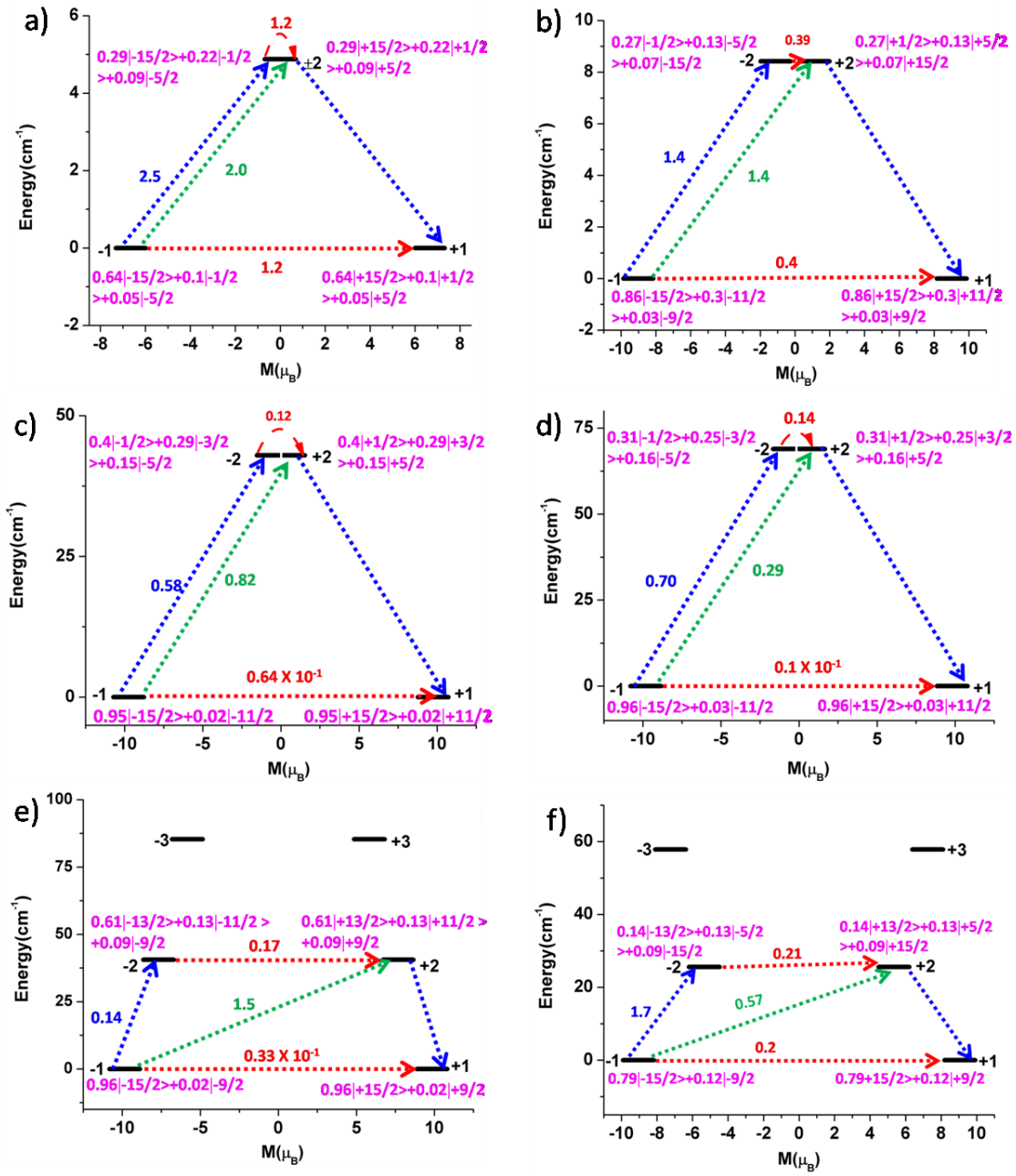

Figure 7. The *ab initio* computed magnetization blocking barrier for a) the Dy1 site in **1**; b) the Dy2 site in **1**; c) the Dy1 site in **2**; d) the Dy2 site in **2**; e) the Dy1 site in **3** and f) the Dy2 site in **3**. The x-axis indicates the magnetic moment of each state along main magnetic axis of Dy ions while y-axis denotes the energy of the respective states. The thick black line indicates the Kramer's doublets as a function of computed magnetic moment. The green/blue arrows show the possible pathway via Orbach/Raman relaxation. The dotted red lines represent the presence of QTM/TA-QTM between the connecting pairs. The numbers provided at each arrow are the mean absolute value for the corresponding matrix element of transition magnetic moment. The numbers given in magenta corresponds to wave function analysis of the m_J levels, where for example, 0.95|-15/2>+0.02|-9/2> indicate that the ground state is pure m_J = ±15/2 with a slight mixing (0.02) with an m_J = 9/2 excited state.

Although the Cr^{III}-Cr^{III} (J_3) exchange is a next-nearest-neighbour interaction, this interaction has previously been highlighted as being important in order to reproduce the low temperature susceptibility data and, therefore has been taken into consideration.[38]

The estimated exchange coupling parameters for complexes **1**-**3** are shown in Table 2 (see Figure 2 for the fit obtained using the POLY_ANISO routine). For complex **1**, the Dy^{III}-Dy^{III} magnetic exchange interaction is found to be antiferromagnetic (-0.16 cm^{-1}) in nature. The average Dy-O-Dy angle in complex **1** is 111.3°. Based on previously developed magneto-structural correlations for

{$Gd^{III}(OR)_2Gd^{III}$} dimers, this angle falls in the antiferromagnetic exchange region.[29b] DFT calculations also reproduce the sign of the exchange interaction affirming this point. For complex **2**, the POLY_ANISO fit yielded a ferromagnetic coupling interaction (1.6 cm^{-1}). Here the average Dy^{III}-O-Dy^{III} angle is found to be 107.8°, while the average Dy^{III}-F-Dy^{III} angle is 113.8°. The above mentioned magneto-structural correlation predicts ferromagnetic exchange coupling for angles below ~107° and this is consistent with the present observation. The magnitude of the exchange interaction, however, is relatively strong compared to other 4f-4f interactions (usually <0.01 cm^{-1}) and this can be traced to the presence of the fluoride bridges, which promote strong polarization (see Figure S6 in ESI).

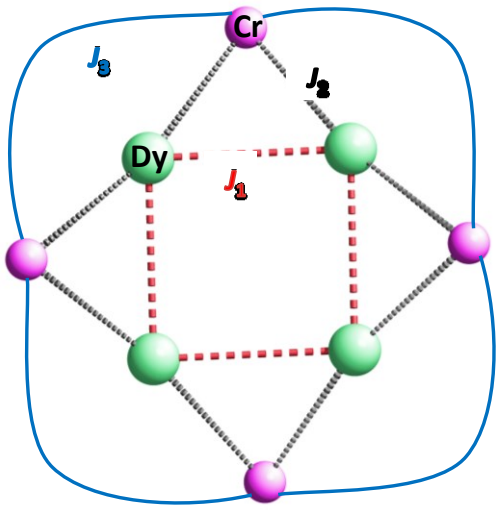

Figure 8. Magnetic exchange pathways in **1**-**3**.

Table 2. Magnetic exchange interactions (cm^{-1}) between magnetic ions in **1**–**3**. *zJ* is a cluster-cluster interaction.

Complex	Magnetic Exchange Interactions (Lines model, in cm^{-1})				Magnetic Exchange Interactions(DFT calculated, in cm^{-1})		
	J_1	J_2	J_3	z*J*	J_1	J_2	J_3
1	-0.16			-0.01	-0.11		
2	1.6			-0.013	0.034		
3	2.8	-1.8	0.005	-0.017	0.02	-0.8	0.005

For complex **3**, the J_1 interaction between the Dy^{III}-Dy^{III} ions is found to be ferromagnetic as observed in **2**. In this case the exchange is even stronger with a magnitude of 2.8 cm^{-1}. The average Dy^{III}-O-Dy^{III} angle is found to be 105.5°, while the average Dy^{III}-F-Dy^{III} angle is 118.5°. Again relating to the {$Gd(OR)_2Gd$} magneto-structural correlation, Dy^{III}-O-Dy^{III} angles smaller than ~107° result in ferromagnetic coupling, with the stronger coupling witnessd in **3** correlating to the smaller angle compared to **2**. Furthermore, as the Dy^{III}-Cr^{III} interaction is determined to be antiferromagnetic this offers another route for stronger ferromagnetic Dy^{III}...Dy^{III} coupling via spin polarization, as evidenced earlier in polynuclear {3d-Gd} complexes.[38]

The Dy^{III}-Cr^{III} interaction is estimated to be antiferromagnetic in nature (-1.8 cm^{-1} by POLY_ANISO and -0.8 cm^{-1} by DFT, based on {$Cr^{III}Gd^{III}$} models). We have previously undertaken detailed mechanistic studies on {$3d(OR)_2Gd$} pairs, as well as fluoride bridged {Cr^{III}-Gd^{III}} pairs.[39] Conclusions from this work are that the magnetic exchange coupling in {3d-4f} pairs has two contributions. A ferromagnetic contribution arising from the charge transfer from a 3d orbital to empty 5d/6s orbitals of Dy^{III} and 4f orbitals contributing to the empty 5d/6s orbitals via polarization as revealed earlier. [38b] The second contribution being an antiferromagnetic contribution resulting from the direct overlap between the 3d SOMOs and the 4f SOMOs. Particularly, unpaired electrons in σ-type d_z^2 and $d_{x^2-y^2}$ orbitals contribute significantly to charge transfer, leading to dominating ferromagnetic contributions, while the remaining π-orbitals tend to overlap with the 4f orbitals. In the case of Cr^{III} possessing the t_{2g}^3 configuration, the charge transfer pathway is negligible and significant overlap with the 4f orbitals is expected, as has been documented.[6c, 39] In **3**, the Dy^{III}-Cr^{III} interaction is mediated by two alkoxide bridges and one carboxylate bridge. Extensive magneto-structural correlations developed for {$Cu^{II}Gd^{III}$}, {$Ni^{II}Gd^{III}$}, {$V^{IV}Gd^{III}$}, {$Cr^{III}Gd^{III}$} and {$Fe^{III}Gd^{III}$} complexes suggest that, for this exchange topology, the coupling is expected to be antiferromagnetic for bridge angles smaller than 105°. Here the Dy^{III}-O-Cr^{III} angles are 103.4 and 98.4°. These relatively small angles enforced in the polynuclear framework promote antiferromagnetic coupling and this is expected to be relative strong, as one of the prominent ferromagnetic contributions will be negligible, as discussed above. These mechanistic arguments are supported by the DFT calculations (See Figure S6).

Magnetic relaxation in the polynuclear framework: For compound **1** the tunnelling (Δ_{tun}) parameter for the exchanged coupled ground state is computed to be large (2.4 $x10^{-3}$, see Figure 9a), but is determined, however, to be very small for **2** (4.4 x 10^{-6}, see Figure 9c) and **3** (4.0 x 10^{-7}, see Figure 9b). Thus, in complex **1** the magnetic relaxation occurs via the ground state with a small energy barrier of 0.001 cm^{-1} (See Table S6 and Figure 9a). In **2**, the first excited state also possesses negligible tunnel splitting, suggesting magnetization blockade up to 3.6 cm^{-1}. The second excited exchange-coupled state lies at 4.0 cm^{-1} (See Table S10 and Figure 9c) and possesses a tunnel splitting of Δ_{tun}= 2.8 $x10^{-4}$ cm^{-1}, which suggests a possible relaxation pathway via this state. Further to this, another relaxation pathway at higher excited states, is expected, with an energy barrier of 49.1 cm^{-1}, possessing significant tunnel splitting (Δ_{tun}= 1.1 $x10^{-5}$, see Table S10). Although the relaxation is expected to occur via the states that lie at 4.0 cm^{-1}, the tunnel splitting for these states are relatively small and minor perturbations such as intermolecular interactions can quench this tunnelling process and could push up the relaxation barrier via higher excited states lying at 49.1 cm^{-1}. This picture is consistent with the experimental data where several relaxation processes are observed, one at very low temperatures with a small the barrier height (2-4 cm^{-1}, estimated) and one at higher temperatures, with a barrier height of 39 cm^{-1} (experimental).

In contrast, for **3**, the tunnelling probability of the ground, first and second excited states are almost negligible, a consequence of stronger Dy^{III}...Dy^{III} and Cr^{III}..Dy^{III} interactions, which quench the QTM leading to relaxation via the third exited state. This places the estimate of U_{cal} for this molecule as 38.0 cm^{-1} (Δ_{tun} =1.4 $x10^{-4}$, see Table S14 and Figure 9b) which is consistent with the experimental data (55 cm^{-1}).[15] Clearly, here only one relaxation is observed unlike in **2**, this suggests that the presence of Cr^{III} ions quench the

low temperature relaxation channel, which was available for the complex **2**.

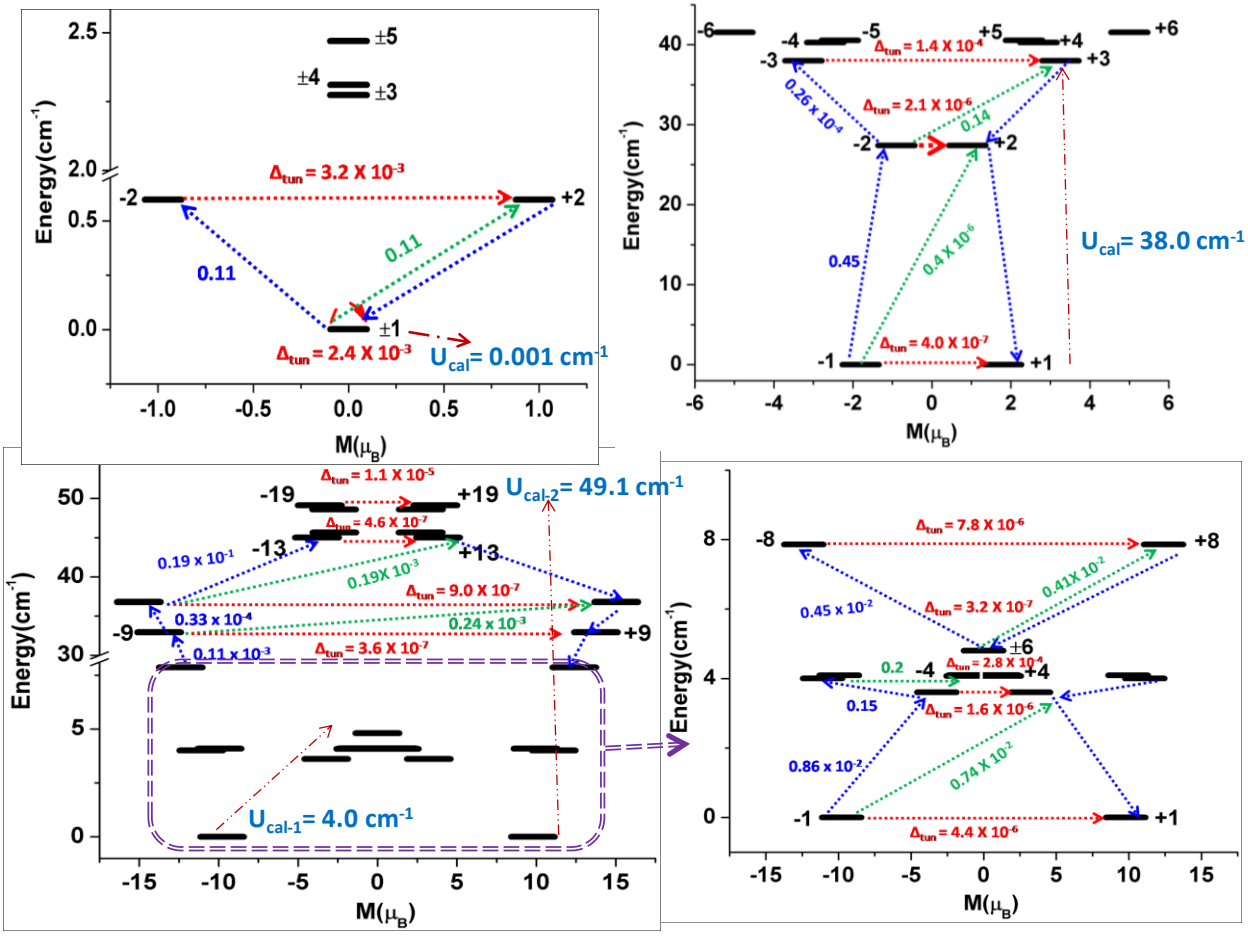

Figure 9. Low-lying exchange spectrum and the position of the magnetization blocking barrier of **1**(a), **3**(b) and **2**(c). The exchange states are placed on the diagram according to their magnetic moments (bold black lines).

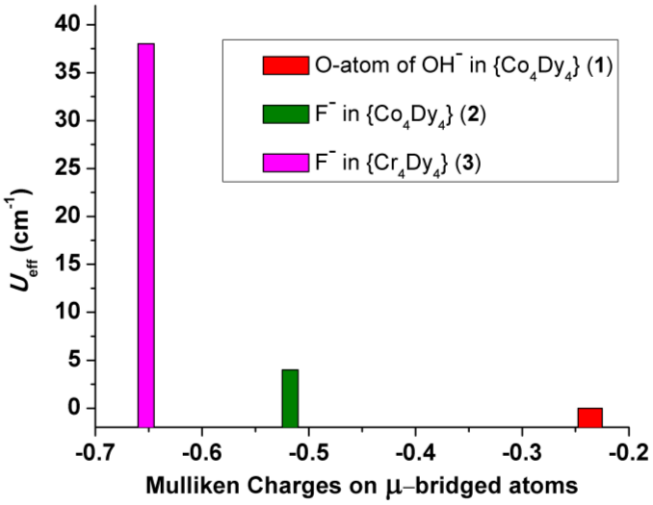

Figure 10. Plot of observed U_{eff} values in $\{TM^{III}_4Dy^{III}_4\}$ vs. Mulliken charge on bridged atoms.

The barrier heights for magnetization reversal are found to be (**1**, 0.001 cm^{-1}) < (**2**, 4.0 cm^{-1}) < (**4**, 10.4 cm^{-1}) < (**3**, 38.0 cm^{-1}).[40] The observed trend clearly suggests that the presence of the F^- ion (**2** (F^-) vs **1** (OH^-) and **3** (F^-) vs **4** (N_3^-)) instigates structural and electronic changes that help to quench the QTM to a certain extent. This is clear if we compare complexes **1** and **2**, where **1** is experimentally not an SMM, while complex **2** exhibits slow relaxation, however, with prominent QTM at lower temperatures. Although the F^- ions help to quench the tunnelling compared to the hydroxide ions present in **1**, we still find a significant tunnel splitting of the exchanged coupled excited state in complex **2** ($2.8x\ 10^{-4}$ cm^{-1}). Complex **4** on the other hand incorporates the paramagnetic Cr^{III} ion, which induces notable exchange coupling between the Cr^{III}-Dy^{III} and Dy^{III}-Dy^{III} ions, quenching the QTM effects. Here, even with bridging hydroxide and azide ligands, QTM is quenched efficiently. This is attributed to relatively strong Dy^{III}-Cr^{III} magnetic exchange interactions. Secondly, if both F^- and Cr^{III} are present, such as in complex **3**, this is doubly effective, where both factors work additively to quench the QTM leading to the observation of a very large barrier for magnetization reversal, and ultimately resulting in

coercive magnetic hysteresis loops, with a blocking temperature of 3.5 K (Figure S5). Our calculations reveal that the electrostatic potential experienced by the ions upon replacement of OH^- by F^- is significant and alters the direction of the ground state magnetic anisotropy. As the F^- ions carry a larger negative charge compare to the hydroxide ions, the barrier heights are found to also correlate to the computed Mulliken charges residing on the bridging atoms (see Figure 10 and Tables S15–S17 and Figures S7–S9 in the Supporting Information).

Conclusion

In summary, we report the synthesis, magnetic and theoretical studies of two analogous heterometallic $\{Co^{III}_4Dy^{III}_4\}$ octanuclear complexes of formulae $[Co^{III}_4Dy^{III}_4(\mu\text{-}OH)_4(\mu_3\text{-}OMe)_4(O_2CC(CH_3)_3)_4(tea)_4(H_2O)_4]\cdot 4H_2O$ (**1**) and $[Co^{III}_4Dy^{III}_4(\mu\text{-}F_4)(\mu_3\text{-}OH)_4(o\text{-}tol)_8(mdea)_4]\cdot 3H_2O\cdot EtOH\cdot MeOH$ (**2**)). Both complexes display the same metallic core topology, with minor structural modifications found in the ligand framework. The major structural difference, in the context of the magnetic behaviour, being the introduction of $\mu\text{-}F^-$ bridging ions for **2**, replacing $\mu\text{-}OH^-$ ions for **1**. We also included in this study a theoretical perspective of two analogous $\{Cr^{III}_4Dy^{III}_4\}$ octanuclear complexes, which display an identical metallic core topology to that of **1** and **2** - $[Cr^{III}_4Dy^{III}_4(\mu\text{-}F_4)(\mu_3\text{-}OMe)_{1.25}(\mu_3\text{-}OH)_{2.75}(O_2CPh)_8(mdea)_4]$ (**3**) and $[Cr^{III}_4Dy^{III}_4(\mu_3\text{-}OH)_4(\mu\text{-}N_3)_4(mdea)_4\ (piv)_4]$(**4**). Compounds **3** and **4** provide a similar O vs F bridging ligand comparison to **1** and **2** (in this case N vs F), but also reveal insight of the influence the 3d transition metal ion has on the magnetic behaviour, when comparing between (**1** and **2**) and (**3** and **4**). The magnetic relaxation data for **1** and **2** (TM = Co^{III}), are found to be significantly different, as are the data for **3** and **4** (TM = Cr^{III}). Further to this, the behaviour of the $\{Co^{III}_4Dy^{III}_4\}$ complexes are notably different from the $\{Cr^{III}_4Dy^{III}_4\}$ complexes. From the ac data, only out-of-phase (χ_M'') "tails" are visible, above 2 K, for **1**, however, **2** exhibits a significant out-of-phase component, revealing multiple relaxation process, the slowest of which revealing a barrier height of 39 cm^{-1}.

Ab initio calculations suggest major differences are found even at single ion level, where the presence of F^- is found to diminish the tunnelling probability of the ground state KDs. In the case of hydroxide bridged complexes, the ground state tunnelling is significantly larger and we show compound **1** and **4** are "worse" SMMs than **2** and **3**. The presence of the F^- ions alters the direction of the magnetic anisotropy and more importantly pushes the first excited state higher in energy due to stronger electrostatic repulsion. This reduces the mixing of the ground m_J = 15/2 with the first excited m_J= 1/2 state leading to reduced QTM effects for the F^- compounds.

At the polynuclear level the presence of weak Dy^{III}-Dy^{III} interactions is strong enough already to quench the QTM completely in complex **2** leading to the observation of SMM behavior, while it is insufficient in complex **1** rendering no SMM characteristics. Furthermore, F^- also influences the exchange coupling, where the Dy^{III}-Dy^{III} coupling is determined to be ten times larger for complex **2** compared to complex **1** (-0.16 cm^{-1} vs. 1.6 cm^{-1} for **1** and **2**, respectively), reiterating further the superiority of F^- over OH^- as a bridging ligand.

Replacement of (diamagnetic) Co^{III} by the paramagnetic d^3 Cr^{III} ion opens up further exchange pathways, where stronger Dy^{III}...Cr^{III} interactions are detected leading to further quenching of the QTM pathways. This is especially so in complex **3** where both Cr^{III} and F^- are present and both factors contribute, additively, to the quenching of QTM leading to the observation of a very large barrier height for magnetization reversal and long relaxation times as observed in the magnetic hysteresis plot.

Acknowledgements

K.S.M thanks the Australian Research Council (ARC) and K.S.M and G.R thank the Australia-India Strategic Research Fund (AISRF) for support of this work. KRV is thankful to the IITB-Monash Research Academy for a PhD studentship. The authors thank Dr Boujemaa Moubaraki for help with magnetism. Structural aspects of this research were undertaken on the MX1 beamline at the Australian Synchrotron, Clayton, Victoria, Australia.

REFERENCES

[1] a) R. Sessoli, D. Gatteschi, A. Caneschi, M. A. Novak, *Nature* **1993**, *365*, 141-143; b) M. Evangelisti, E. K. Brechin, *Dalton Trans.* **2010**, *39*, 4672-4676.

[2] a) R. A. Layfield, *Organometallics* **2014**, *33*, 1084-1099; b) D. N. Woodruff, R. E. P. Winpenny, R. A. Layfield, *Chem. Rev.* **2013**, *113*, 5110-5148; c) P. Zhang, Y.-N. Guo, J. Tang, *Coord. Chem. Rev.* **2013**, *257*, 1728-1763.

[3] a) D. Gatteschi, R. Sessoli, J. Villain, *Molecular Nanomagnets*, Oxford University Press, Oxford, **2006**; b) D. Gatteschi, *Adv. Mater.* **1994**, *6*, 635-645.

[4] a) J. D. Rinehart, M. Fang, W. J. Evans, J. R. Long, *J. Am. Chem. Soc.* **2011**, *133*, 14236-14239; b) J. D. Rinehart, M. Fang, W. J. Evans, J. R. Long, *Nat. Chem.* **2011**, *3*, 538-542.

[5] S. K. Gupta, T. Rajeshkumar, G. Rajaraman, R. Murugavel, *Chem. Sci.* **2016**, *7*, 5181-5191.

[6] a) N. F. Chilton, *Inorg. Chem.* **2015**, *54*, 2097-2099; b) S. Sanz, J. M. Frost, T. Rajeshkumar, S. J. Dalgarno, G. Rajaraman, W. Wernsdorfer, J. Schnack, P. J. Lusby, E. K. Brechin, *Chem. Eur. J.* **2014**, *20*, 3010-3013; c) K. S. Pedersen, G. Lorusso, J. J. Morales, T. Weyhermüller, S. Piligkos, S. K. Singh, D. Larsen, M. Schau-Magnussen, G. Rajaraman, M. Evangelisti, J. Bendix, *Angew. Chem. Int. Ed.* **2014**, *53*, 2394-2397; d) K. R. Vignesh, S. K. Langley, K. S. Murray, G. Rajaraman, *Chem. Eur. J.* **2015**, *21*, 2881-2892; e) T. Pugh, N. F. Chilton, R. A. Layfield, *Angew. Chem. Int. Ed.* **2016**, *55*, 11082-11085.

[7] L. Sorace, C. Benelli, D. Gatteschi, *Chem. Soc. Rev.* **2011**, *40*, 3092-3104.

[8] J. D. Rinehart, M. Fang, W. J. Evans, J. R. Long, *J. Am. Chem. Soc.* **2011**, *133*, 14236-14239.

[9] a) S. K. Singh, T. Gupta, G. Rajaraman, *Inorg. Chem.* **2014**, *53*, 10835-10845; b) T. Pugh, V. Vieru, L. F. Chibotaru, R. A. Layfield, *Chem. Sci.* **2016**, *7*, 2128-2137; c) T. Pugh, F. Tuna, L. Ungur, D. Collison, E. J. L. McInnes, L. F. Chibotaru, R. A. Layfield, *Nat. Commun.* **2015**, *6*, 7492.

[10] a) N. F. Chilton, D. Collison, E. J. L. McInnes, R. E. P. Winpenny, A. Soncini, *Nat. Commun.* **2013**, *4*; b) I. Oyarzabal, J. Ruiz, E. Ruiz, D. Aravena, J. M. Seco, E. Colacio, *Chem. Commun.* **2015**, *51*, 12353-12356; c) J. D. Rinehart, J. R. Long, *Chem. Sci.* **2011**, *2*, 2078-2085.

[11] R. E. P. Winpenny, in *Perspectives in Supramolecular Chemistry*, John Wiley & Sons, Ltd., **1999**, pp. 193-223.

[12] F. Habib, G. Brunet, V. Vieru, I. Korobkov, L. F. Chibotaru, M. Murugesu, *J. Am. Chem. Soc.* **2013**, *135*, 13242-13245.

[13] a) S. K. Langley, N. F. Chilton, B. Moubaraki, K. S. Murray, *Chem. Commun.* **2013**, *49*, 6965-6967; b) S. K. Langley, N. F. Chilton, B. Moubaraki, K. S. Murray, *Inorg. Chem.* **2013**, *52*, 7183-7192; c) S. K. Langley, N. F. Chilton, B. Moubaraki, K. S. Murray, *Inorg. Chem. Front.* **2015**, *2*, 867-875; d) S. K. Langley, N. F. Chilton, L. Ungur, B. Moubaraki, L. F. Chibotaru, K. S. Murray, *Inorg. Chem.* **2012**, *51*, 11873-11881; e) S. K. Langley, C. Le, L. Ungur, B. Moubaraki, B. F. Abrahams, L. F. Chibotaru, K. S. Murray, *Inorg. Chem.* **2015**, *54*, 3631-3642; f) S. K. Langley, L. Ungur, N. F. Chilton, B. Moubaraki, L. F. Chibotaru, K. S. Murray, *Inorg. Chem.* **2014**, *53*, 4303-4315.

[14] a) J. P. Costes, S. Titos-Padilla, I. Oyarzabal, T. Gupta, C. Duhayon, G. Rajaraman, E. Colacio, *Chem. Eur. J.* **2015**, *21*, 15785-15796; b) J. P. Costes, S. Titos-Padilla, I. Oyarzabal, T. Gupta, C. Duhayon, G. Rajaraman, E. Colacio, *Inorg. Chem.* **2016**, *55*, 4428-4440; c) A. Upadhyay, S. K. Singh, C. Das, R. Mondol, S. K. Langley, K. S. Murray, G. Rajaraman, M. Shanmugam, *Chem. Commun.* **2014**, *50*, 8838-8841.

[15] S. K. Langley, C. M. Forsyth, B. Moubaraki, K. S. Murray, *Dalton Trans.* **2015**, *44*, 912-915.

[16] J. Rinck, G. Novitchi, W. Van den Heuvel, L. Ungur, Y. Lan, W. Wernsdorfer, C. E. Anson, L. F. Chibotaru, A. K. Powell, *Angew. Chem. Int. Ed.* **2010**, *49*, 7583-7587.

[17] N. P. Cowieson, D. Aragao, M. Clift, D. J. Ericsson, C. Gee, S. J. Harrop, N. Mudie, S. Panjikar, J. R. Price, A. Riboldi-Tunnicliffe, R. Williamson, T. Caradoc-Davies, *J. Synchrotron Radiat.* **2015**, *22*, 187-190.

[18] T. M. McPhillips, S. E. McPhillips, H.-J. Chiu, A. E. Cohen, A. M. Deacon, P. J. Ellis, E. Garman, A. Gonzalez, N. K. Sauter, R. P. Phizackerley, S. M. Soltis, P. Kuhn, *J. Synchrotron Radiat.* **2002**, *9*, 401-406.

[19] W. Kabsch, *J. Appl. Crystallogr.* **1993**, *26*, 795-800.

[20] G. Sheldrick, *Acta Crystallogr. Sect. A* **2008**, *64*, 112-122.

[21] G. M. Sheldrick, *SHELXL-97, Programs for X-ray Crystal Structure Refinement;* **1997**, University of Göttingen: Göttingen, Germany, .

[22] L. J. Barbour, *J. Supramol. Chem.* **2001**, *1*, 189-191.

[23] F. Aquilante, T. B. Pedersen, V. Veryazov, R. Lindh, *WIREs Comput. Mol. Sci.* **2013**, *3*, 143-149.

[24] L. F. Chibotaru, L. Ungur, *J. Chem. Phys.* **2012**, *137*, 064112-064122.

[25] L. F. Chibotaru, L. Ungur, *Program POLY_ANISO* **2006**, *University of Leuven*.

[26] L. Noodleman, *J. Am. Chem. Soc.* **1981**, *74*, 5737-5743.

[27] a) S. Piligkos, G. Rajaraman, M. Soler, N. Kirchner, J. van Slageren, R. Bircher, S. Parsons, H.-U. Gudel, J. Kortus, W. Wernsdorfer, G. Christou, E. K. Brechin, *J. Am. Chem. Soc.* **2005**, *127*, 5572-5580; b) G. Rajaraman, J. Cano, E. K. Brechin, E. J. L. McInnes, *Chem. Commun.* **2004**, 1476-1477; c) E. Ruiz, J. Cano, S. Alvarez, P. Alemany, *J. Comput. Chem.* **1999**, *20*, 1391-1400; d) E. Ruiz, J. Cano, S. Alvarez, A. Caneschi, D. Gatteschi, *J. Am. Chem. Soc.* **2003**, *125*, 6791-6794; e) E. Ruiz, A. Rodríguez-Fortea, J. Cano, S. Alvarez, P. Alemany, *J. Comput. Chem.* **2003**, *24*, 982-989.

[28] a) N. Berg, T. Rajeshkumar, S. M. Taylor, E. K. Brechin, G. Rajaraman, L. F. Jones, *Chem. Eur. J.* **2012**, *18*, 5906-5918; b) S. Ghosh, S. K. Singh, S. Tewary, G. Rajaraman, *Dalton Trans.* **2013**, *42*, 16490-16493; c) G. Rajaraman, M. Murugesu, E. C. Sanudo, M. Soler, W. Wernsdorfer, M. Helliwell, C. Muryn, J. Raftery, S. J. Teat, G. Christou, E. K. Brechin, *J. Am. Chem. Soc.* **2004**, *126*, 15445-15457.

[29] a) T. Rajeshkumar, G. Rajaraman, *Chem. Commun.* **2012**, *48*, 7856-7858; b) S. K. Singh, T. Rajeshkumar, V. Chandrasekhar, G. Rajaraman, *Polyhedron* **2013**, *66*, 81-86.

[30] a) M. L. Baker, G. A. Timco, S. Piligkos, J. S. Mathieson, H. Mutka, F. Tuna, P. Kozlowski, M. Antkowiak, T. Guidi, T. Gupta, H. Rath, R. J. Woolfson, G. Kamieniarz, R. G. Pritchard, H. Weihe, L. Cronin, G. Rajaraman, D. Collison, E. J. L. McInnes, R. E. P. Winpenny, *Proc. Natl. Acad. Sci. USA* **2012**, *109*, 19113-19118; b) P. Christian, G. Rajaraman, A. Harrison, M. Helliwell, J. J. W. McDouall, J. Raftery, R. E. P. Winpenny, *Dalton Trans.* **2004**, 2550-2555; c) P. Christian, G. Rajaraman, A. Harrison, J. J. W. McDouall, J. T. Raftery, R. E. P. Winpenny, *Dalton Trans.* **2004**, 1511-1512; d) G. Rajaraman, E. Ruiz, J. Cano, S. Alvarez, *Chem. Phys. Lett.* **2005**, *415*, 6-9.

[31] W. Liu, H. H. Thorp, *Inorg. Chem.* **1993**, *32*, 4102-4105.

[32] C. Benelli, D. Gatteschi, *Chem. Rev.* **2002**, *102*, 2369-2388.

[33] B. N. Figgis, *Introduction to Ligand Fields*, Wiley, New York, **1966**.

[34] a) J. Cirera, E. Ruiz, S. Alvarez, *Chem. Eur. J.* **2006**, *12*, 3162-3167; b) M. Pinsky, D. Avnir, *Inorg. Chem.* **1998**, *37*, 5575-5582.

[35] H. L. C. Feltham, Y. Lan, F. Klöwer , L. Ungur, L. F. Chibotaru, A. K. Powell, S. Brooker, *Chem. Eur. J.* **2011**, *17*, 4362-4365.

[36] a) K. R. Vignesh, S. K. Langley, B. Moubaraki, K. S. Murray, G. Rajaraman, *Chem. Eur. J.* **2015**, *21*, 16364-16369; b) C. Das, S. Vaidya, T. Gupta, J. M. Frost, M. Righi, E. K. Brechin, M. Affronte, G. Rajaraman, M. Shanmugam, *Chem. Eur. J.* **2015**, *21*, 15639-15650.

[37] S. K. Langley, D. P. Wielechowski, V. Vieru, N. F. Chilton, B. Moubaraki, B. F. Abrahams, L. F. Chibotaru, K. S. Murray, *Angew. Chem. Int. Ed.* **2013**, *52*, 12014-12019.

[38] a) S. K. Singh, M. F. Beg, G. Rajaraman, *Chem. Eur. J.* **2016**, *22*, 672-680; b) S. K. Singh, N. K. Tibrewal, G. Rajaraman, *Dalton Trans.* **2011**, *40*, 10897-10906.

[39] S. K. Singh, K. S. Pedersen, M. Sigrist, C. A. Thuesen, M. Schau-Magnussen, H. Mutka, S. Piligkos, H. Weihe, G. Rajaraman, J. Bendix, *Chem. Commun.* **2013**, *49*, 5583-5585.

[40] Note: the quoted values are U_{cal} values except for complex **4** where U_{eff} value is given.